BPCC: Design of a hybrid Bioinspired model for improving efficiency of PPGClassification under Clinical scenarios

Mrs. Neha Singh*, Dr. Arun Kumar[2], Ms. Divya Singh[3]

[1] Research Scholar, Dept. of ETC, BIT, Durg (C.G.), India and neha.singh@bitdurg.ac.in

[2] Professor and Head, Dept Of ETC, BIT, Durg (C.G.), India and arun.kumar@bitdurg.ac.in

[3]Research Scholar, Dept. of Biomedical Eng., NIT, Raipur (C.G.), India and divya.twinks@gmail.com

Abstract: Photoplethysmography (PPG) signals are used for preliminary analysis of heart diseases via processing of optical measurements. Existing methods for classification of PPG signals are either highly complex to deploy, or have lower accuracy levels, which limits their clinical applicability under real-time scenarios. To overcome these issues, this text proposes design of a novel hybrid bioinspired model for improving efficiency of PPG classification under clinical scenarios. The proposed model initially collects temporal PPG signals, and extracts Frequency & Gabor features for multidomain representations. These signals are processed via a hybrid Genetic Particle Swarm Optimizer (GPSO), that assists in identification of correlative features for different disease types. These temporal correlative features are used to find different diseases with higher efficiency, and lower complexity levels. Due to which the proposed model is able to identify Arrythmia, High Blood Pressure, and Myocardial Infraction conditions with 3.4% higher accuracy, 2.9% higher precision, 2.5% higher recall, and 8.3% lower delay when compared with existing methods.

Keywords: PPG, Classification, Heart, Issues, Myopathy, Arrythmia, Multidomain, GPSO, Process

DOI: 10.53555/ecb/2022.11.10.217

1. Introduction

Numerous physiological parameters, such as heart rate [1, 2], blood oxygen saturation via Neural Architecture Search (NAS) [2, 3], blood pressure via semi-classical signal analysis (SSSA) [4, 5], and respiratory rate [6, 7], have been evaluated using the photoplethysmography (PPG) signal. Non-invasive photoplethysmography uses optical techniques such as transmission or reflection, as shown in Figure 1. The low-intensity infrared light emitted by an LED on the skin is largely absorbed by veins and arteries. The quantity of light that was not absorbed is determined by the reflection PPG by using backscattered light, which is seen by a photo diode. The LED and photo diode are co-mounted, as illustrated in Figure 1a. The unabsorbed light will be collected by the transmission PPG and then detected by a photo diode. As shown in Figure 1b, the LED and photo diode are situated on opposing sides. The PPG signal may be utilized to monitor changes in blood volume using reflection or transmission methods, notwithstanding its limitations as a quantitative indicator (Figure 1). Compared to the signal

recorded by transmission, the PPG signal measured via reflection is more prone to distortion brought on by motion noise. Currently, a wearable device's PPG sensor is used to monitor physiological data using a technique based on reflection. PPG signals may have motion artifacts when users are utilizing these devices while moving, such as while running and other movements.

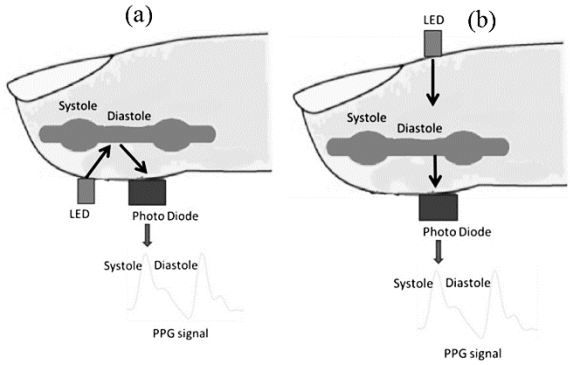

Figure 1 (a). The reflective sensing process, (b) Refractive sensing process

Device mechanics are often changed to improve measurement accuracy and reduce the effect of motion on the recoded PPG signal. However, more accurate measurements will be made of the parameters obtained from a PPG signal of a certain quality. This makes understanding how to categorize PPG signal quality a critical obstacle to be solved in the creation of wearable technology. Changes in blood volume and the physiological responses to these events in peripheral arteries may be measured using non-invasive optical monitoring techniques like PPG. Its waveform therefore exhibits traditional morphological characteristics [7,8]. A PPG pulse contains physiological features such the primary peak, dicrotic notch, pulse width, and amplitude, as shown in Figure 2. These critical elements have been used by several research to evaluate the quality of each PPG pulse (i.e., rule-based techniques). The SQI also shows how warped the PPG pulse really is. Work in [10] employed a decision tree and aspects of the PPG waveform, while [9] used fuzzy rules to classify the SQI of PPG pulses. Work in [11] used the Bayesian method of assessing hypotheses to analyze the SQI. The rule-based approach's criteria must be adjusted to suit each unique situation in order to get the best results in these investigations. Recently, [12] used a fuzzy neural network to study the SQI. The rule-based method was utilized to filter out the PPG pulses that were significantly polluted, while artificial intelligence was used to assess clean PPG pulses. Taking traits out of the PPG signal is a step in the traditional evaluation process for SQI. It is common knowledge that the morphological approach is vulnerable to signal noise and has a number of drawbacks in terms of the performance resilience of the classification model [8]. Today, deep learning techniques are used to solve convolutional feature extraction tasks [13].

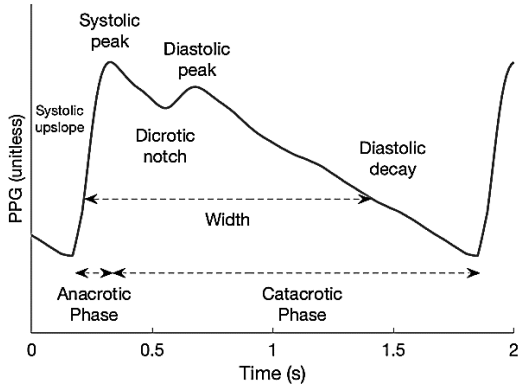

Figure 2. Components of PPG signals

Since one-dimensional signals are what physiological data like electrocardiograms, electroencephalograms, and Photoplethysmogram (PPGs) are, many studies [14, 15] have used a one-dimensional deep convolution neural network (1D DCNN) to

distinguish between various types of arrhythmias and the signal's quality. Numerous studies [16, 17, 18] have shown that wavelet transforms, short time frequency transforms, and power spectral densities may be used to transform a 1D signal into a 2D signal. These images were sent to the 2D DCNN for classification. In contrast, in these tests a 2- to 5-second signal fragment was transformed into a visual representation. As a result, the algorithms could only handle steady, continuous data. During the systolic phase of the pulse, the amount of blood pumped into the body's circulatory system is measured; this volume is referred to as the stroke volume (SV). During this time, the thoracic cavity's volume will change. Work in [19] proposes using impedance cardiography to non-invasively measure cardiac hemodynamic parameters (ICG) via Wavelet and CNN (WCNN). When ICG technology is employed, LVET, which is determined by the ICG signal, is an essential part of the SV calculation. ICG transmissions have a low signal-to-noise ratio, which makes LVET ineffective. The LVET was measured by Liu et al. [a reflecting PPG sensor positioned on the neck] in [5]. PPG pulses more accurately identified LVETs when compared to ICG pulses, according to research. Consequently, the recommended approach's SV measurement accuracy was improved in comparison to the conventional ICG method. A higher signal-to-noise ratio (SQI) in the PPG signal, as previously mentioned, leads to more accurate assessments of the underlying physiological parameters. The clinical relevance of current methods for real-time categorization of PPG signals is limited by their implementation difficulties or lower levels of accuracy. The following chapter of this book makes a suggestion for the development of a special hybrid bioinspired model to overcome these issues and improve the effectiveness of PPG classification in clinical settings. Section 3 calculates the model's effectiveness and evaluates it against other models in terms of accuracy, precision, recall, and delay metrics using data from large-scale validation. The authors provide clinical findings on the proposed paradigm at the end of the study along with recommendations for strengthening its deployment in real-time use cases.

2. Design of the proposed hybrid bioinspired model for improving efficiency of PPG classification under clinical scenarios

Based on the review of existing PPG classification techniques, it can be observed that these methods are either highly complex to deploy, or have lower accuracy levels, which limits their clinical applicability under real-time scenarios.

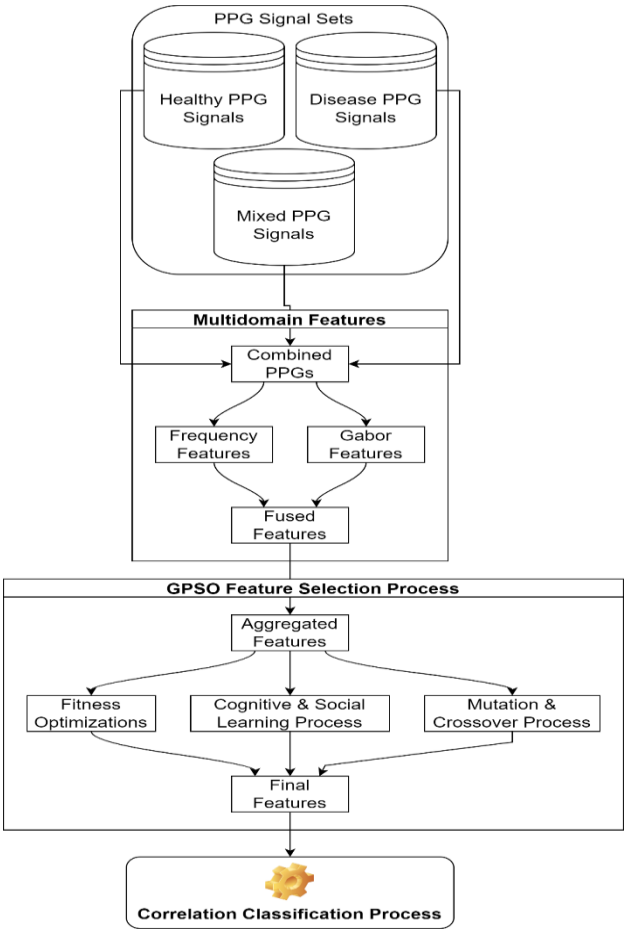

Figure 3. Design of the proposed PPG classification process

To overcome these issues, this section discusses design of a novel hybrid bioinspired model for improving efficiency of PPG classification under clinical scenarios. Design of the proposed model is depicted in figure 3, where it can be observed that the proposed model initially collects temporal PPG signals, and extracts Frequency & Gabor features for multidomain representations. These signals are processed via a hybrid Genetic Particle Swarm Optimizer (GPSO), that assists in identification of correlative features for different disease types. These temporal correlative features are used to find different diseases with higher efficiency, and lower complexity levels. Due to which the proposed model is able to identify Arrythmia, High Blood Pressure, and Myocardial Infraction conditions.

To perform this task, the model initially estimates Fourier features from input PPG signals via equation 1,

$$DFT_i = \sum_{j=1}^{N_f} x_j * \left[cos\left(\frac{2*\pi*i*j}{N_f}\right) - \sqrt{-1} * sin\left(\frac{2*\pi*i*j}{N_f}\right)\right] \dots (1)$$

Where, x represents the input PPG signal values, while N_f represents total number of PPG features. These features are cascaded with a Gabor feature analysis process, that assists in estimation of spatial features via equation 2,

$$G(x,y)_s = e^{\frac{-x`^2+\partial^2*y'^2}{2*\emptyset^2}} * \cos\left(2*\frac{pi}{\lambda}*x'\right) \dots (2)$$

Where, ∂ & $\emptyset$ are the angular ranges used for spatial analysis, and can be in the range of $(0,2\pi)$, while x & y are the sample number and its intensity levels. These levels are augmented via equations 3 & 4 as follows,

$$x' = x * \cos(\phi) + y * \sin(\phi) \dots (3)$$
$$y' = -x * \sin(\phi) + y * \cos(\phi) \dots (4)$$

Thee values are combined to form a PPG Feature Vector (PPFV), which might contain inherent redundancies due to extraction of similar feature sets. To reduce this redundancy, a Genetic Particle Swarm Optimizer (GPSO) Model is used, which assists in retaining highly variant feature sets. The GPSO model works as per the following process,

- Initially, for setting up the optimizer, the following constants are set as per designer choices,

- Count of particles which will be generated (N_p)
- Count of solutions that will be reconfigured (N_s)
- Rate of mutation for learning (L_r)
- Social & Cognitive learning factors (L_c & L_s)

- A set of N_p particles are initially generated via the following operations
  - Select N stochastic features via equation 5,

$$N = STOCH(L_r * N(PPFV), N(PPFV)) \dots (5)$$

Where, $N(PPFV)$ are the total features present in the PPFV feature sets, and $STOCH$ is a stochastic Markovian process.

  - As per these features, estimate their particle fitness levels via equation 6,

$$f_h = \frac{t_p}{t_p + t_n} \dots (6)$$

Where, t_p & t_n are the correct and incorrect classification counts.

  - Repeat this process for N_p particles, and then estimate a particle fitness threshold via equation 7,

$$f_{th} = \frac{1}{N_p} \sum_{i=1}^{N_p} f_i * L_r \dots (7)$$

- Based on this estimation, iterate through N_i iterations, and generate N_s solutions via the following process,
  - If current particle fitness is $f > f_{th}$, then store it for future operations
  - Else modify its fitness via equation 7,

$$f(New) = f(Old) + L_s\big(f(Old) - f(Best)\big) + L_c\Big(f(Old) - f\big(Best_p\big)\Big) \dots (7)$$

Where, $f(Best)$ is the highest fitness of all particles, while $f(Best_p)$ is the highest fitness of current particle in previous iterations.

  - Stochastically modify the features so that fitness of current solution is $f(New)$

- This process is repeated for N_i iterations, and particle with highest fitness is selected for feature evaluation operations.

For every new input, these operations are repeated, and its class is estimated w.r.t. old inputs via an efficient correlation process. This process estimates Pearson Correlation via equation 8 between all new input features, and existing feature sets.

$$C = \frac{\sum_{i=1}^{N_{sel}} \begin{pmatrix} x_i - \\ avg(x) \end{pmatrix} \begin{pmatrix} x(New)_i \\ -avg(x(New)) \end{pmatrix}}{\sqrt{\sum_{i=1}^{N_{sel}} \begin{pmatrix} x_i - \\ avg(x) \end{pmatrix}^2 \sum_{i=1}^{N_{sel}} \begin{pmatrix} x(New)_i \\ -avg(x(New)) \end{pmatrix}^2}} \dots (8)$$

Where, x & $x(New)$ are the existing training features & new input feature sets. Output class for this new sample is estimated for maximum value of correlation, and is used to identify different disease types. Due to which the model is able to categorize PPG signals into multiple disease categories. Validation of this model is

done in the next section of this text, where its efficiency is compared with existing techniques in terms of accuracy, precision & recall levels for different scenarios.

3. Comparative analysis of the proposed model under different scenarios

The proposed model uses a multidomain feature representation process in order to estimate Fourier and Gabor feature sets. These feature sets are selected by a fusion of Genetic Algorithm & Particle Swarm Optimization, which assists in identification of high efficiency feature values, that can increase true-positive rates, while reducing false classifications. The selected features are correlated with existing sample sets, which assists in classification of input samples into different disease categories. Efficiency of this model was evaluated in terms of accuracy (A), precision (P), recall (R), and delay (d) needed for classification w.r.t. NAS [2], SSSA [5], and WCNN [19] techniques. This efficiency was estimated on Biobank (https://www.ukbiobank.ac.uk/), Medical Information Mart for Intensive Care (https://mimic.mit.edu/), Vital DB (https://vitaldb.net/), MIMIC PERform Datasets (https://zenodo.org/record/6973963#.Y6bKoHZBy3A), Physionet Data Samples https://physionet.org/content/pulse-transit-time-ppg/1.1.0/), and Real World PPG Data Samples (https://data.mendeley.com/datasets/yynb8t9x3d/3), which were combined to form a total of 1 million records. Out of these records, 80% were used for training the model, while remaining 10% each were used for testing & validation purposes. Based on this strategy, the accuracy of classification w.r.t. different Testing Sample Sets (TSS), can be observed from table 1 as follows,

TTS	**A (%) NAS [2]**	**A (%) SSSA [5]**	**A (%) WCNN [19]**	**A (%) BPCC**
1000	92.95	84.74	89.02	95.00
2000	93.08	84.96	89.54	95.31
3000	93.14	85.22	90.02	95.60
5000	93.23	85.46	90.41	95.85
10000	93.32	85.69	90.83	96.12
20000	93.42	85.93	91.23	96.38
25000	93.53	86.16	91.67	96.67
30000	93.63	86.40	92.18	96.97
40000	93.73	86.64	92.62	97.25
45000	93.83	86.87	93.07	97.53
50000	93.93	87.11	93.52	97.82
55000	94.04	87.35	93.97	98.10
60000	94.14	87.59	94.42	98.38
70000	94.24	87.82	94.87	98.66
80000	94.34	88.06	95.32	98.94
90000	94.43	88.30	95.77	99.23
100000	94.53	88.53	96.22	99.51

Table 1. Classification accuracy for different input samples

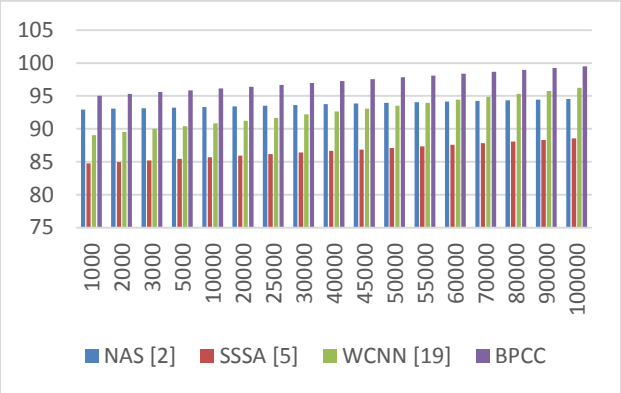

Figure 4. Classification accuracy for different input samples

As per this evaluation and figure 4, it can be observed that the proposed model is capable of improving the accuracy of classification by 4.9% when compared with NAS [2], 8.3% when compared with SSSA [5], and 3.5% when compared with WCNN [19] under different scenarios. This improvement is due to use of multidomain feature sets along with bioinspired modelling for selection of high efficiency feature sets. Similar to this evaluation, the precision can be observed from table 2 as follows,

TTS	**P (%) NAS [2]**	**P (%) SSSA [5]**	**P (%) WCNN [19]**	**P (%) BPCC**
1000	87.24	79.66	83.93	89.35
2000	87.33	79.89	84.37	89.61
3000	87.40	80.12	84.77	89.87
5000	87.49	80.34	85.14	90.11
10000	87.58	80.56	85.54	90.37
20000	87.68	80.78	85.96	90.63
25000	87.78	81.00	86.40	90.90
30000	87.88	81.22	86.83	91.17
40000	87.97	81.45	87.25	91.44
45000	88.06	81.67	87.68	91.70
50000	88.16	81.89	88.10	91.97
55000	88.25	82.11	88.52	92.23
60000	88.34	82.34	88.94	92.50
70000	88.44	82.56	89.36	92.76
80000	88.53	82.78	89.78	93.02
90000	88.62	83.00	90.20	93.29
100000	88.71	83.23	90.62	93.55

Table 2. Classification precision for different input samples

As per this evaluation and figure 5, it can be observed that the proposed model is capable of improving the precision of classification by 4.5% when compared with NAS [2], 9.5% when compared with SSSA [5], and 2.9% when compared with WCNN [19] under different scenarios. This improvement in precision is due to use of multidomain feature sets along with correlative analysis for identification of different disease classes.

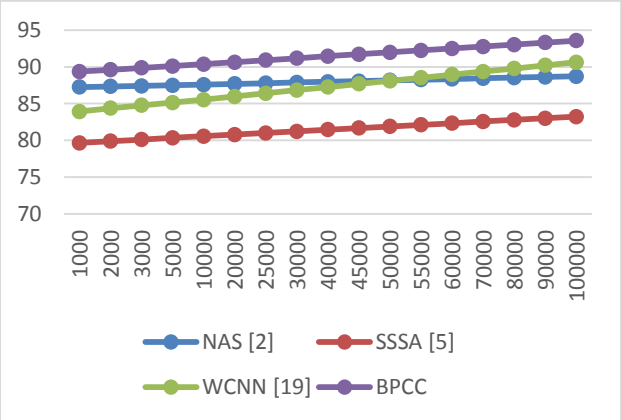

Figure 5. Classification precision for different input samples

Similar to this evaluation, the recall can be observed from table 3 as follows,

TTS	**R (%) NAS [2]**	**R (%) SSSA [5]**	**R (%) WCNN [19]**	**R (%) BPCC**
1000	91.29	83.36	87.81	93.48
2000	91.38	83.59	88.28	93.77
3000	91.46	83.83	88.70	94.03
5000	91.55	84.06	89.10	94.29
10000	91.65	84.29	89.51	94.55
20000	91.75	84.52	89.94	94.83
25000	91.85	84.76	90.40	95.12
30000	91.95	84.99	90.86	95.40
40000	92.05	85.22	91.30	95.68
45000	92.15	85.45	91.74	95.96
50000	92.25	85.68	92.18	96.23
55000	92.35	85.92	92.62	96.51
60000	92.44	86.15	93.06	96.79
70000	92.54	86.39	93.50	97.06
80000	92.64	86.62	93.94	97.34
90000	92.73	86.85	94.38	97.61
100000	92.83	87.08	94.82	97.89

Table 3. Classification recall for different input samples

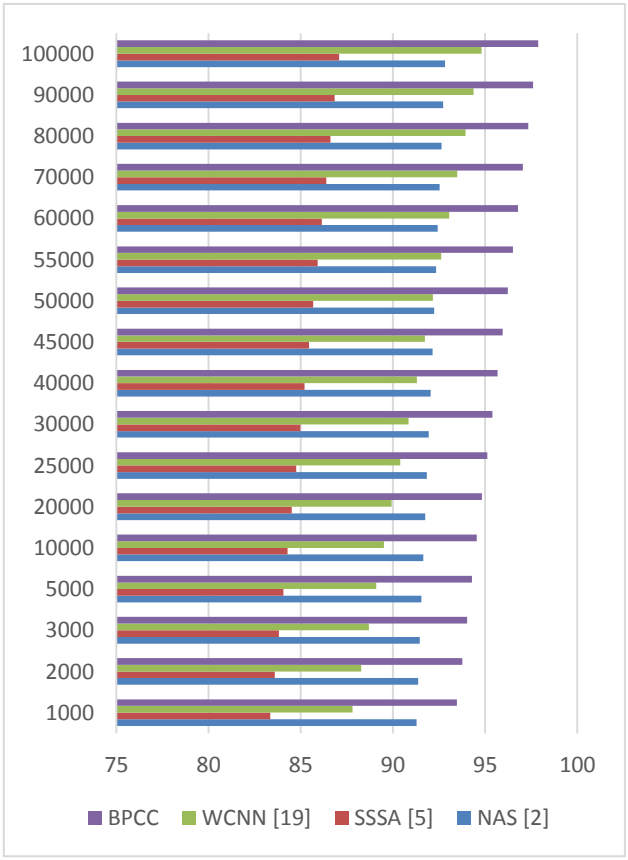

Figure 6. Classification recall for different input samples

As per this evaluation and figure 6, it can be observed that the proposed model is capable of improving the recall of classification by 5.5% when compared with NAS [2], 10.4% when compared with SSSA [5], and 1.5% when compared with WCNN [19] under different scenarios. This improvement in recall is due to use of multidomain feature sets & bioinspired computing along with correlative analysis for identification of different disease classes. Similarly, the delay can be observed from table 4 as follows,

TTS	**D (ms) NAS [2]**	**D (ms) SSSA [5]**	**D (ms) WCNN [19]**	**D (ms) BPCC**
1000	120.20	99.29	112.51	93.48
2000	120.32	99.57	113.11	93.77
3000	120.42	99.86	113.64	94.03
5000	120.54	100.13	114.15	94.29
10000	120.67	100.41	114.68	94.55
20000	120.80	100.68	115.23	94.83
25000	120.94	100.96	115.82	95.12
30000	121.07	101.24	116.41	95.40
40000	121.20	101.51	116.98	95.68
45000	121.33	101.79	117.54	95.96
50000	121.46	102.06	118.11	96.23
55000	121.59	102.34	118.67	96.51
60000	121.72	102.62	119.23	96.79
70000	121.85	102.90	119.80	97.06
80000	121.97	103.18	120.36	97.34
90000	122.10	103.45	120.93	97.61
100000	122.23	103.73	121.49	97.89

Table 4. Delay needed to classify different sample sets

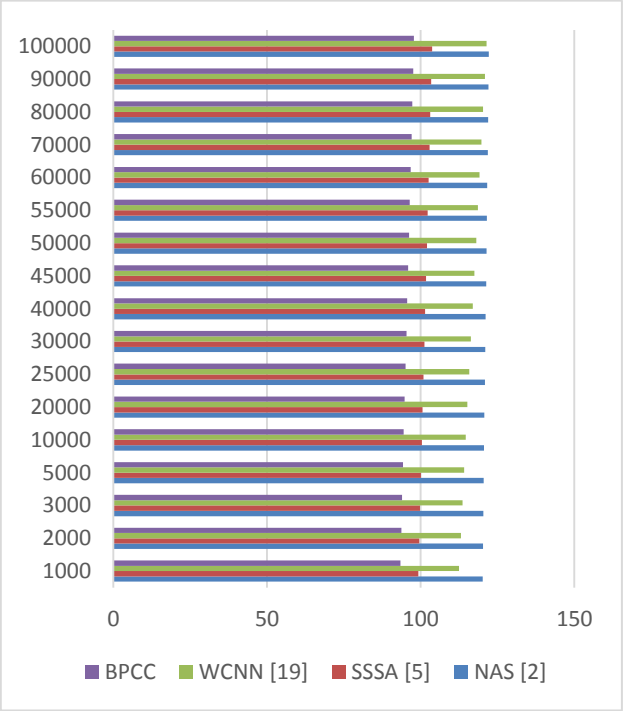

Figure 7. Delay needed to classify different sample sets

As per this evaluation and figure 7, it can be observed that the proposed model is capable of improving the speed of classification by 19.5% when compared with NAS [2], 8.3% when compared with SSSA [5], and 18.5% when compared with WCNN [19] under different scenarios. This improvement in speed is due to use of bioinspired computing for processing of

multidomain feature sets. Due to these improvements, the model is capable of deployment to a wide variety of clinical scenarios.

4. Conclusion and Future Scope

Using a multidomain feature representation method, the proposed model estimates Fourier and Gabor feature sets. These feature sets are chosen using a combination of Genetic Algorithm and Particle Swarm Optimization, which aids in identifying high-efficiency feature values that can increase true-positive rates while decreasing false classifications. The selected characteristics are correlated with existing sample sets, which facilitates the categorization of input samples into various disease categories. In terms of classification accuracy, it was observed that the proposed model can improve classification accuracy by 4.9% when compared to NAS [2], 8.3% when compared to SSSA [5], and 3.5% when compared to WCNN [19] in various scenarios. This improvement is attributable to the utilization of multidomain feature sets in conjunction with bioinspired modeling for the selection of high-efficiency feature sets. In terms of classification consistency, it was observed that the proposed model is capable of improving classification precision by 4.5% compared to NAS [2], 9.5% compared to SSSA [5], and 2.9% compared to WCNN [19] under various conditions. This increase in accuracy is attributable to the use of multidomain feature sets and correlative analysis for the identification of various disease classes. When evaluated in terms of consistency levels, it was discovered that the proposed model is capable of enhancing the recall of classification by 5.5% when compared to NAS [2], 10.4% when compared to SSSA [5], and 1.5% when compared to WCNN [19] under various conditions. This improvement in recall is attributable to the utilization of multidomain feature sets, bioinspired computing, and correlative analysis for identifying distinct disease classes. In terms of classification delay, it was observed that the proposed model is able to improve classification speed by 19.5% when compared to NAS [2], 8.3% when compared to SSSA [5], and 18.5% when compared to WCNN [19] under various conditions. This acceleration is a result of the use of bioinspired computing to process multidomain feature sets. Due to these enhancements, the model is deployable in a vast array of clinical scenarios.

In the future, this model's performance must be validated on larger data sets, and it can be enhanced through the incorporation of deep transfer learning models for multimodal analysis. These models may consist of Generative Adversarial Networks (GANs) and Auto Encoders (AEs), among others. This performance can also be enhanced through the incorporation of high-complexity bio-inspired techniques that aid in the pre-emption and dynamic selection of multiple feature sets.

Authors Contribution

Mrs. Neha Singh*. Research Scholar BIT, DURG developed the theory, collected the data and performed the analytical and computations work and also develops the draft of manuscript.

Dr. Arun Kumar, Head and professor BIT, DURG give proper guidance during analytical work and critically revised the manuscript

Mrs. Divya Singh Research Scholar NIT, Raipur also develop computational work of the research and revised the manuscript

All authors contributed to the study conception and design. Material preparation, data collection, and analysis were done by all the authors. All authors read and approved the final version of the current manuscript.

Declarations

Corresponding author Mrs. Neha Singh, Research Scholar, Dept. of ETC, BIT, Durg

Consent to Participate Each potential participant was informed about the design and objectives of the study,

Consent for Publication: As the Patients is not signed with any other consent organization so there is no need of taking consent for publication. The authors declare no competing interests

Conflict of Interest The authors declare no competing interests.

Funding: Any opinions, findings, conclusions, or recommendations expressed in this material are those of the authors and do not necessarily reflect the views of the funders.

5. References

[1] G. N. K. Reddy, M. S. Manikandan and N. V. L. N. Murty, "Evaluation of Objective Distortion Measures for Automatic Quality Assessment of Processed PPG Signals for Real-Time Health Monitoring Devices," in IEEE Access, vol. 10, pp. 15707-15745, 2022, doi: 10.1109/ACCESS.2022.3148256.

[2] S. B. Song, J. W. Nam and J. H. Kim, "NAS-PPG: PPG-Based Heart Rate Estimation Using Neural Architecture Search," in IEEE Sensors Journal, vol. 21, no. 13, pp. 14941-14949, 1 July1, 2021, doi: 10.1109/JSEN.2021.3073047.

[3] A. Burrello et al., "Q-PPG: Energy-Efficient PPG-Based Heart Rate Monitoring on Wearable Devices," in IEEE Transactions on Biomedical Circuits and Systems, vol. 15, no. 6, pp. 1196-1209, Dec.2021,doi: 10.1109/TBCAS.2021.3122017.

[4] K. Natarajan et al., "Photoplethysmography Fast Upstroke Time Intervals Can Be Useful Features for Cuff-Less Measurement of Blood Pressure Changes in Humans," in IEEE Transactions on Biomedical Engineering, vol. 69, no. 1, pp. 53-62, Jan. 2022, doi: 10.1109/TBME.2021.3087105.

[5] P. Li and T. -M. Laleg-Kirati, "Central Blood Pressure Estimation From Distal PPG Measurement Using Semiclassical Signal Analysis Features," in IEEE Access, vol. 9, pp. 44963-44973, 2021, doi: 10.1109/ACCESS.2021.3065576.

[6] Q. Lin et al., "A 134 DB Dynamic Range Noise Shaping Slope Light-to-Digital Converter for Wearable Chest PPG Applications," in IEEE Transactions on Biomedical Circuits and Systems, vol. 15, no. 6, pp. 1224-1235, Dec. 2021, doi: 10.1109/TBCAS.2021.3130470.

[7] D. Y. Hwang, B. Taha and D. Hatzinakos, "PBGAN: Learning PPG Representations From GAN for Time-Stable and Unique Verification System," in IEEE Transactions on Information Forensics and Security, vol. 16, pp. 5124-5137, 2021, doi: 10.1109/TIFS.2021.3122817.

[8] M. Salah, O. A. Omer, L. Hassan, M. Ragab, A. M. Hassan and A. Abdelreheem, "Beat-Based PPG-ABP Cleaning Technique for Blood Pressure Estimation," in IEEE Access, vol. 10, pp. 55616-55626, 2022, doi: 10.1109/ACCESS.2022.3175436.

[9] S. Gupta, A. Singh, A. Sharma and R. K. Tripathy, "Higher Order Derivative-Based Integrated Model for Cuff-Less Blood Pressure Estimation and Stratification Using PPG Signals," in IEEE Sensors Journal, vol. 22, no. 22, pp. 22030-22039, 15 Nov.15, 2022, doi:

10.1109/JSEN.2022.3211993.

[10] S. Haddad, A. Boukhayma and A. Caizzone, "Continuous PPG-Based Blood Pressure Monitoring Using Multi-Linear Regression," in IEEE Journal of Biomedical and Health Informatics, vol. 26, no. 5, pp. 2096-2105, May 2022, doi: 10.1109/JBHI.2021.3128229.

[11] H. Wang, P. Kang, Q. Gao, S. Jiang and P. B. Shull, "A Novel PPG-FMG-ACC Wristband for Hand Gesture Recognition," in IEEE Journal of Biomedical and Health Informatics, vol. 26, no. 10, pp. 5097-5108, Oct. 2022, doi: 10.1109/JBHI.2022.3194017.

[12] S. Heo, S. Kwon and J. Lee, "Stress Detection With Single PPG Sensor by Orchestrating Multiple Denoising and Peak-Detecting Methods," in IEEE Access, vol. 9, pp. 47777-47785, 2021, doi: 10.1109/ACCESS.2021.3060441.

[13] J. I. Rodriguez-Labra, C. Kosik, D. Maddipatla, B. B. Narakathu and M. Z. Atashbar, "Development of a PPG Sensor Array as a Wearable Device for Monitoring Cardiovascular Metrics," in IEEE Sensors Journal, vol. 21, no. 23, pp. 26320-26327, 1 Dec.1, 2021, doi: 10.1109/JSEN.2021.3064219.

[14] S. Hinatsu, N. Matsuda, H. Ishizuka, S. Ikeda and O. Oshiro, "Identification of PPG Measurement Sites Toward Countermeasures Against Biometric Presentation Attacks," in IEEE Access, vol. 10, pp. 118736-118746, 2022, doi: 10.1109/ACCESS.2022.3221456.

[15] D. Y. Hwang, B. Taha, D. S. Lee and D. Hatzinakos, "Evaluation of the Time Stability and Uniqueness in PPG-Based Biometric System," in IEEE Transactions on Information Forensics and Security, vol. 16, pp. 116-130, 2021, doi: 10.1109/TIFS.2020.3006313.

[16] R. K. Pandey and P. C. . -P. Chao, "A Dual-Channel PPG Readout System With Motion-Tolerant Adaptability for OLED-OPD Sensors," in IEEE Transactions on Biomedical Circuits and Systems, vol. 16, no. 1, pp. 36-51, Feb. 2022, doi: 10.1109/TBCAS.2021.3138996.

[17] S. Gupta, A. Singh, A. Sharma and R. K. Tripathy, "dSVRI: A PPG-Based Novel Feature for Early Diagnosis of Type-II Diabetes Mellitus," in IEEE Sensors Letters, vol. 6, no. 9, pp. 1-4, Sept. 2022, Art no. 7003404, doi: 10.1109/LSENS.2022.3203609.

[18] O. Mazumder, R. Banerjee, D. Roy, S. Bhattacharya, A. Ghose and A. Sinha, "Synthetic PPG Signal Generation to Improve Coronary Artery Disease Classification: Study With Physical Model of Cardiovascular System," in IEEE Journal of Biomedical and Health Informatics, vol. 26, no. 5, pp. 2136-2146, May 2022, doi: 10.1109/JBHI.2022.3147383.

[19] Jiaze Wu, Hao Liang, Changsong Ding, Xindi Huang, Jianhua Huang, Qinghua Peng, "Improving the Accuracy in Classification of Blood Pressure from Photoplethysmography Using Continuous Wavelet Transform and Deep Learning", *International Journal of Hypertension*, vol. 2021, Article ID 9938584, 9 pages, 2021. https://doi.org/10.1155/2021/9938584